# Research on Microseismic Passive Velocity Tomography Based on Template Matching Technology

**Qiankun Zhua, Xingdong Zhaoa**
Department of Mining Engineering, Northeastern University, National Mine Safety Administration, Shenyang, China

**Shawn Boltz, Derrick Chambers**
Spokane Research Lab, National Institute of Occupational Safety and Health

**Erik Westman**
Department of Mining & Minerals Engineering, Virginia Tech

## ABSTRACT

Microseismic passive velocity tomography is becoming an effective technology for large-scale mining-induced stress monitoring in underground mines, especially in the field of early warning of mining-induced hazards. Aiming at the problems of missing low-magnitude events in traditional microseismic monitoring, as well as the potential to increase the resolution of the tomograms in both time and space, a microseismic passive velocity tomography analysis method based on the template matching method was proposed. First, the template matching method was used to pick microseismic events. Then, the probabilistic, non-linear, global-search earthquake location method was used to locate the events and calculate travel time and travel distance. Finally, the fast-marching method was used to carry out passive velocity tomography analysis to image the movement of the abutment stress associated with the longwall. The results show that the selected templates can identify more microseismic events than the traditional microseismic analysis, and the variation trend of events in each day is consistent with the data from the traditional analysis. Using microseismic event locations, travel times and travel distance can effectively complete microseismic passive velocity tomography analysis in each day during the study period and can effectively identify the forward and side abutment stress zones of that longwall panel. This study provides a reference for the identification of mine-induced high stress zones, which has implications for hazard identification and mitigation, with increased resolution of the tomograms in time and space.

## INTRODUCTION

Underground mining activities cause stress redistribution within the surrounding rock, resulting in the formation of high-stress concentration areas in the surrounding rock of panels or roadways (Peng, 2019; Rezaei, 2015). Mining-induced stress concentration is the fundamental cause of surrounding rock instability. Some possible source mechanisms of underground mining-induced seismic events include cavity collapse, pillar burst, tensional fault, normal fault, and thrust faulting (Gibowicz, 1989). The common failure modes are spalling, squeezing, and rockbursts, which seriously restrict the safe and efficient operation of underground mines.

Mining-induced stress analysis methods can be divided into theoretical analysis, numerical simulation, physical modeling, and field monitoring (Xu, 2012). High precision microseismic monitoring has been widely used in metal and non-metal mines for seismic risk identification and mitigation (Young, 1992; Mendecki, 1996; Trifu, 2009). Through microseismic monitoring, we can observe the microseismic events and their information when the surrounding rock deformation and failure occurs in the process of mining-induced stress evolution (Mendecki, 1996). The quantitative parameters of single and groups of microseismic events, such as b-value, energy index, cumulative number of events, focal mechanism, etc., can potentially be used to forecast the stress-induced instability of surrounding rock, and help to understand the mining-induced stress evolution and surrounding rock response characteristics.

Many studies show that there is a corresponding relationship between seismic wave velocity and stress (Wepfer and Christensen, 1991; Khaksar et al., 1999; Zheng et al., 2009). Under various stress states, the ultrasonic wave velocity and stress of sandstone are approximately linearly correlated within a certain range of stress levels (Li, 2013). Nur et al. (1969) found that the P-wave velocity through cylindrical granite samples increased with the increase of stress, and the magnitude of the increase is related to the direction of stress and P-wave propagation. In the field of mining, P-wave velocity has been used to evaluate relative mining-induced stress levels (Maxwell and Young, 1992; Westman, 1993; Luxbacher et

al. 2008). This evaluation process is based on seismic tomography. Under a specific background velocity, the P-wave travel time from sensors to events is used to invert the P-wave velocity of each voxel, and then the evolution law of mining-induced stress can be deduced according to the change of P-wave velocity (Ma et al., 2020; Ghaychi Afrouz, 2020). To summarize the prior work, the quality of the velocity tomography results depends on the accuracy and reliability of arrival time picking, microseismic location, ray tracing, and inversion algorithms. At the same time, the time span should be shortened to improve the time resolution of velocity tomography and provide actionable early warning and prevention information. The inclusion of more events in the inversion results in higher-resolution tomograms that can be obtained with greater frequency.

Match filtering, which is a method of detecting earthquakes or other seismic events based on the similarity between waveforms to known events, has been shown to be effective in the analysis of repeating or near-repeating seismic events, which tend to produce highly similar waveforms (Chambers et al., 2015; Chamberlain et al., 2017). The matched-filter detection method can also be used in the detection of the repeating low-frequency earthquakes (Chamberlain et al., 2014), aftershock detection and analysis (Peng and Zhao, 2009; Yin, 2018; Yin, 2019), detection of the acoustic emission events (Li et al., 2018), mining-induced collapse (Kubacki et al., 2014), and geological structural identification (Spottiswoode and Milev, 1998). More recently, a study has used interferometry and back projection with one month of seismic data collected on the surface above a longwall mine to image mining-induced changes in the overburden (Rabade et al., 2022).

In this paper, the match filtering method was used to pick missing events of the microseismic monitoring system, and the lower quality data were removed by using a repicking method based on the cross-correlation coefficient and the number of stations used for detection. Then the detected events were located by using a probabilistic, non-linear, global-search earthquake location method. The arrival times, travel distances, and event locations were extracted from the event location result files and used to conduct passive P-wave velocity tomography. The tomograms were analyzed to better understand the mining-induced stress change in each day, which shows potential to be used for early warning and hazard prevention in a timely manner.

## DATA

The seismic data set used for this study was collected by a temporary surface geophone network that included 11 three-component geophones. Temporary surface seismic arrays such as this one have been used to provide meaningful data related to changes in the overburden above an active mine (Boltz et al., 2018; Johnson et al., 2021). The geophones were deployed on the surface above the longwall panel, as shown in Figure 1, buried in shallow holes and loosely covered with dirt. Although this study only analyzed data from a 14-day period, each geophone had an internal battery that allowed a 25-day monitoring period. Seismic signals were sampled with a 500 Hz sample rate and 30dB of gain was used.

## METHODS

### 3.1 Event detection

Before conducting template-matching, a group of templates must be generated. We chose 25 original detected events (locations shown in Figure 2) on day 2 of the dataset to make templates, using the "EQcorrscan" code (Chamberlain et al., 2017). The original intention of selecting these 25 events was to cover the magnitude range of all original events as much as possible. The template events were extracted from continuous waveform data, and bandpass filtered between 0.5–20 Hz. Template windows for each channel were 2 seconds long and began 0.10 seconds before the manual pick for the corresponding channel (Figure 3). Only P-phase templates were constructed and only on the vertical channels. The

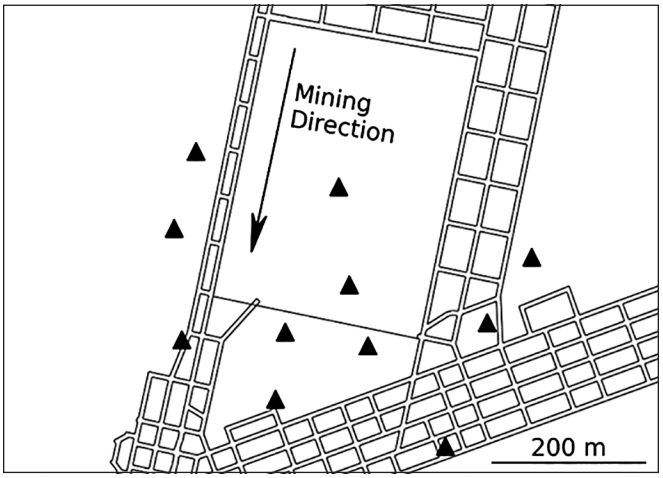


**Figure 1. Plan-view plot of temporary geophone deployment. Triangles represent the geophone locations**

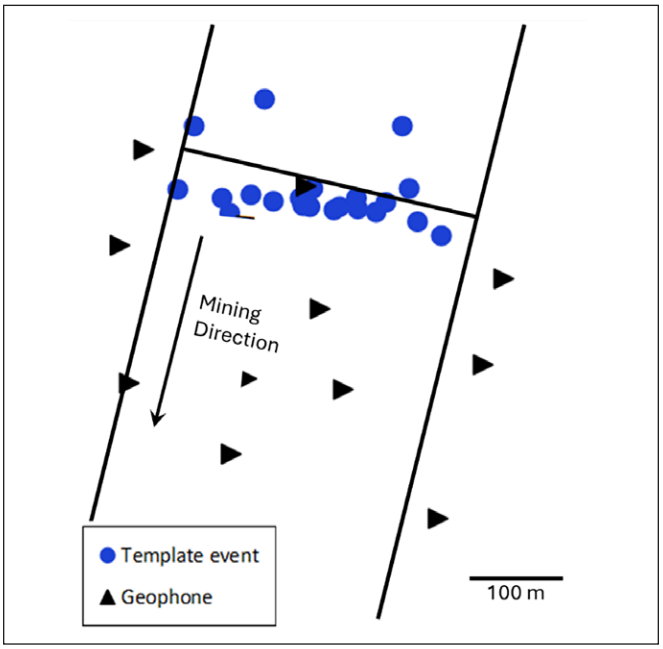


**Figure 2. Distribution of the template events**

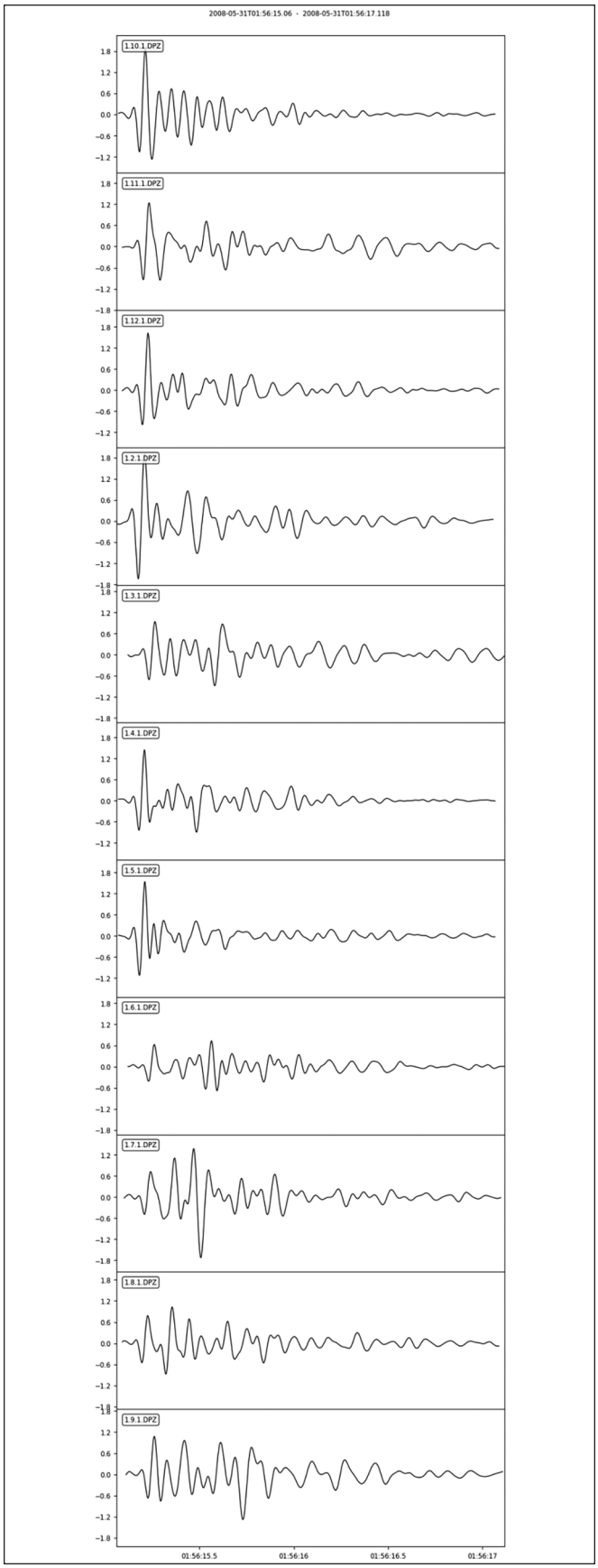


**Figure 3. Waveform of Template 1**

network cross-correlation detection was based on the matched-filter method in EQcorrscan. In this method, the initial templates are correlated with day-long waveforms of the temporary network. All correlation routines within EQcorrscan compute normalized cross correlations according to Equation (1). A function was then used to repick the detected phase data. A minimum cross-correlation coefficient of 0.5 was selected using the time-reversed template method developed by Slinkard et al. (2014) (Figure 4).

$$cc(y) = \frac{\sum_{x=0}^{n}(t(x)-\bar{t})(d(x+y)-\bar{d}(y))}{\sqrt{\sum_{x=0}^{n}(t(x)-\bar{t})^2 \sum_{x=0}^{n}(d(x+y)-\bar{d}(y))^2}} \quad (1)$$

where $cc(y)$ is the normalized cross-correlation coefficient for every sample $y$, $t$ is the template, $n$ is the length of the template, d is the continuous data, $\bar{d}(y)$ is the local mean of the continuous data between sample y and sample $y+n$, and $\bar{t}$ is the mean of the template.

### 3.2 Event Location

The velocity model used for the event locations is based on a regional velocity model for the region surrounding the mine. The uppermost layers of the model were further refined by making manual P- and S-picks on a random subset of events and performing initial event locations. The travel times from the events to a station located 3.5 km away were then used to determine an apparent velocity, assuming the events located at mine level. This assumed that the station was far enough away to minimize the effects of the epicentral location uncertainties of the events on the velocity estimate. The events were relocated with the updated model and the process was then repeated using all stations and fitting a line to the travel times to the temporary stations deployed during this study. The resulting model is shown in Figure 5.

The software code "NonLinLoc" developed by Lomax (2000, 2009), was used to locate the events that were detected with template matching. The NonLinLoc code provides probabilistic, non-linear, global-search seismic event location based on a provided velocity model. The non-linear earthquake location algorithms contained in NonLinLoc follow the probabilistic formulation of inversion in Tarantola and Valette (1982) and Tarantola (1987). The travel times between each geophone and all nodes of an x, y, z grid are calculated using a 3D version of the Eikonal finite-difference scheme of Podvin and Lecomte (1991).

The phase data that were used in the location determination effort were repicked from the original detected data, and only cross-correlation values exceeding 0.5 were used. Based on the assumption that high-quality picks were previously obtained from the cross-correlation absolute picks, and to avoid the potential issue of cycle skipping, the pick time correction was restricted to be within 0.1 seconds.

### 3.3 Tomography

For each event, the arrival time was converted to a travel time by assuming a linear relationship between source-receiver distance and travel time, calculating the intercept, and then subtracting the intercept from each arrival time for the event. Only events with at least 8 rays were used and if the correlation coefficient of any detected event was less than 0.7 the event was discarded. As an example, the resulting scatter plot of source-receiver distance and

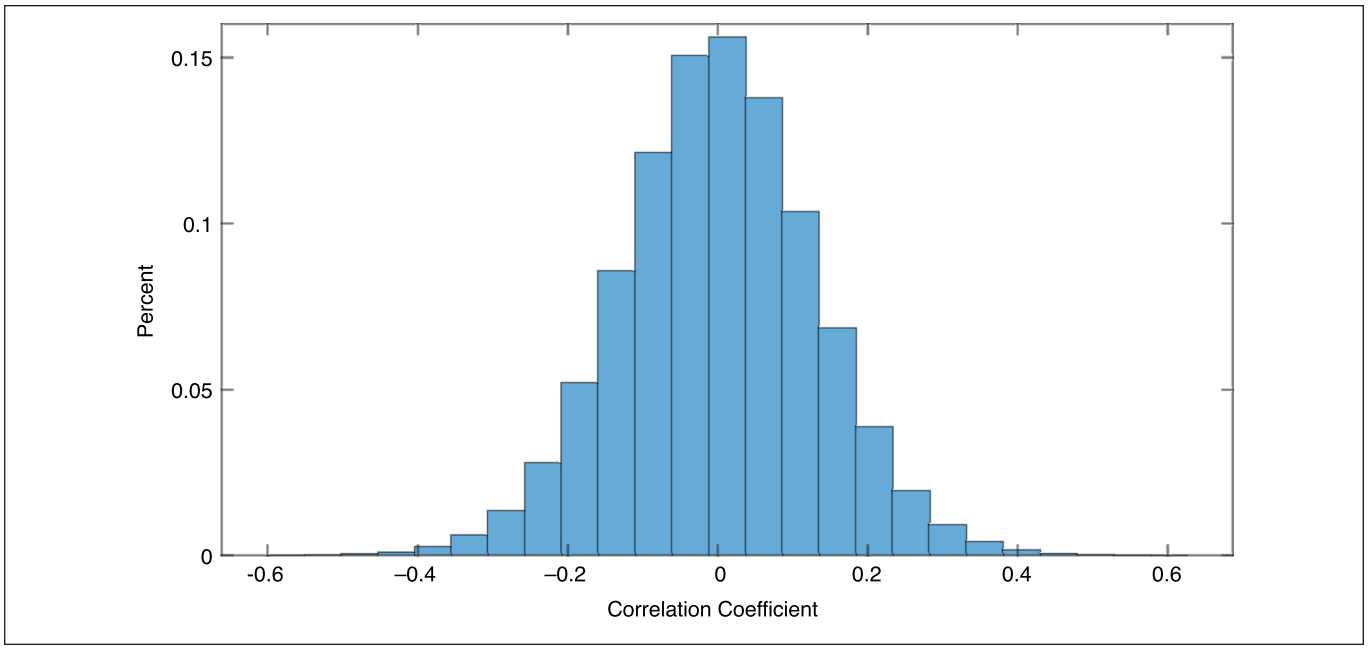


**Figure 4. Actual distribution of the normalized cross-correlation coefficient values from template 1**

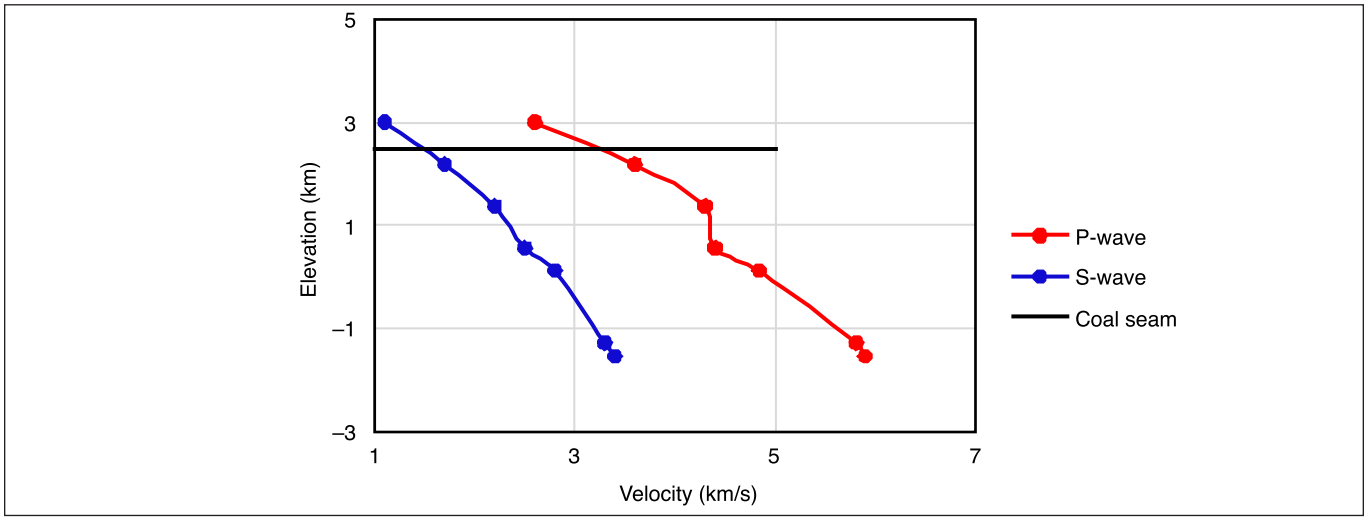


**Figure 5. Background velocity model**

travel time for June 1 is shown as Figure 6. This figure shows that many of the travel times fall along a linear trend of 2,600 m/s, however a substantial number of them lie above that linear trend, these are attributed to either slower travel times due to interactions with the low-velocity gob zone or simply poor picks of the event arrival time.

To invert the travel times into a velocity distribution for the overburden, the fast marching method was used to trace the raypaths and a modified Simultaneous Iterative Reconstruction Technique (SIRT) was used for the inversion. For the tomography calculations an essential component is the calculated travel time from the event to the geophone. For this process the fast marching method was used. The fast marching method is a numerical method for solving the Eikonal equation for wave propagation by getting the finite difference approximation for point in a three-dimensional grid. It is regarded as one of the most accurate and computationally-efficient means for generating raypaths through a velocity model (Sethian, 1996). The initial velocity model was uniform with a velocity of 2,500 m/s. Because the fast marching method performs better when a distribution of velocities exists, an initial iteration with straight rays was conducted. All remaining iterations use the fast marching method to simulate the curved raypaths from source to receiver; travel times for the simulated raypaths were then calculated by summing the distance divided by the velocity between nodes along the path. The voxel size was selected as nine meters per edge to optimize the relationship between resolution and calculation efficiency. Figure 7 shows the sum of the squared differences between calculated and measured travel times for each iteration of the Day 5 data.

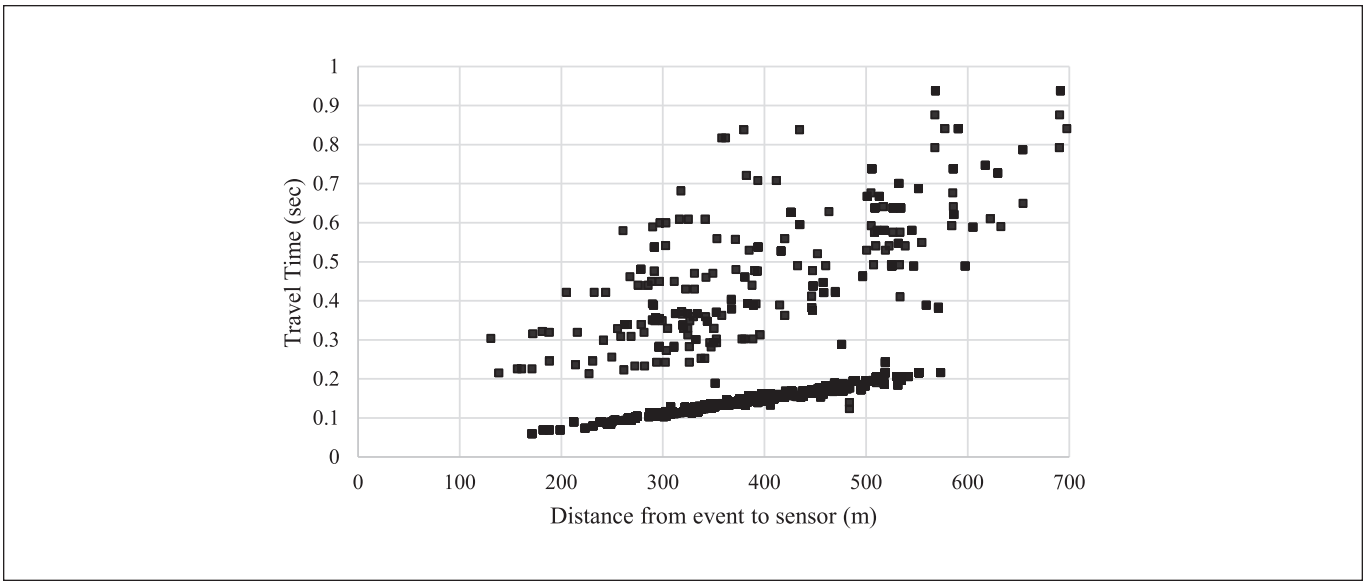


**Figure 6. Scatter plot of source-receiver distance and travel time for Day 3**

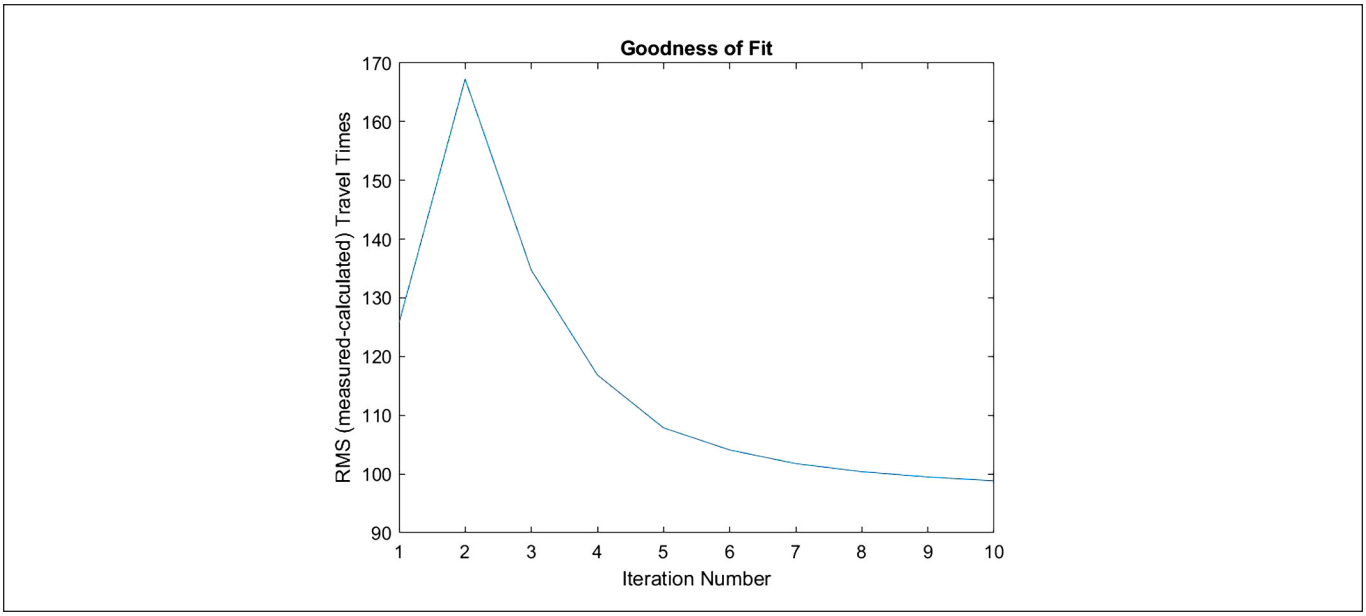


**Figure 7. Relationship between the sum of the squared differences between calculated and measured travel times for each iteration of the Day 5 data**

## RESULTS

### 4.1 Events Detected by Template Matching

Template matching resulted in 17,952 events with arrival times for the 14 days of data，while the number of original detected events is 8,025. Table 1 shows the number of detected events for each day using the matched-filter method and the number of original detected events. These data and the corresponding mining rate (in meters per day) for each day are plotted in Figure 8. As shown in Figure 8, the number of events is correlated to the mining rate; when the mining rate is higher, the number of induced microseismic events is generally higher. The reason for this correlation is that the excavation volume is larger at a higher mining rate and the surrounding rock is disturbed at a larger scale. Day 2 and Day 10 show an elevated number of microseismic events, even though there is no change of mining rate, which may be caused by periodic collapse of the main roof. Another result also can be observed in Figure 8; the variation of microseismic events detected by original and matched-filter method is highly correlated, and the correlation lends confidence to the detector. That is to say, the matched-filter method can effectively detect mining-induced microseismic events with provided templates, and the number of events detected by this method can reflect the mining-induced surrounding rock response characteristics.

**Table 1. Comparison of matched-filter result with original data**

| Day | Original | Matched-filter |
|---|---|---|
| 1 | 214 | 373 |
| 2 | 819 | 1940 |
| 3 | 678 | 1578 |
| 4 | 406 | 1345 |
| 5 | 387 | 1065 |
| 6 | 787 | 1700 |
| 7 | 750 | 2082 |
| 8 | 481 | 1379 |
| 9 | 401 | 1239 |
| 10 | 1016 | 1974 |
| 11 | 407 | 1012 |
| 12 | 294 | 452 |
| 13 | 709 | 918 |
| 14 | 676 | 895 |
| Total | 8,025 | 17,952 |

In Figure 9, the event locations using the NonLinLoc code with phase data from the matched-filter method and original data are plotted for Day 12. Compared with the original data, more events were detected ahead of the working face, which will help to better understand the surrounding rock response better and will help us improve the resolution of the velocity tomography results in both time and space. There is some increased scatter in the locations of the template-detected events, likely due to the new detections being smaller and less well-constrained. The scattered events are only a very small proportion of the dataset, however, and are unlikely to have a significant negative impact on the tomography results.

### 4.2 Tomograms

When a longwall face advances, abutment pressures form around the edges of the gob zone (Figure 10), which will superimpose on abutment zones formed during roadway development. The abutment pressure in front of the face is called the forward abutment pressure, and the abutment pressures along the roadways on both sides of the panel in the gob are the side abutment pressures. Absolute stress level in these abutment zones are always higher than in situ stress. As for the surrounding rock, the roof strata will go through many cycles of caving, including initial caving and periodic caving, which will result in de-stressed zones in the gob area. The tomograms should reflect the process associated with mining-induced stress changes.

The P-wave velocity tomograms were conducted on one-day intervals. The calculated velocity distributions were plotted in Voxler software. An inverse distance to the first power interpolator was used with a grid size of 5 meters and a search radius of 30 meters. In order to check the P-wave velocity distribution caused by mining-induced stress, a section plane was set at the coal seam level. The P-wave velocity variations are shown on the tomograms in Figure 11. Plan views for days 1, 2, 3, 4, 5, 6, 7, 8 are displayed with the working face locations overlain onto the tomograms. In all of these images, the high velocity zone corresponding to the forward abutment is readily visible. This high velocity zone moves south with the advance of the working face, and the area and magnitude of this high velocity zone also changes corresponding to the face movement. In many of these images, a high velocity zone appears which aligns with the headgate and tailgate. According to the distribution of abutment pressure, the high velocity zone should indicate where the high abutment pressure is located, i.e., front abutment pressure and side abutment pressures. Low velocity zones also can be identified in all images which tend to occur on the west side and sometimes can be seen in front of the working face. The range and magnitude are changing with the advance of the working face, but it shows a decreasing trend toward the end of the monitoring period.

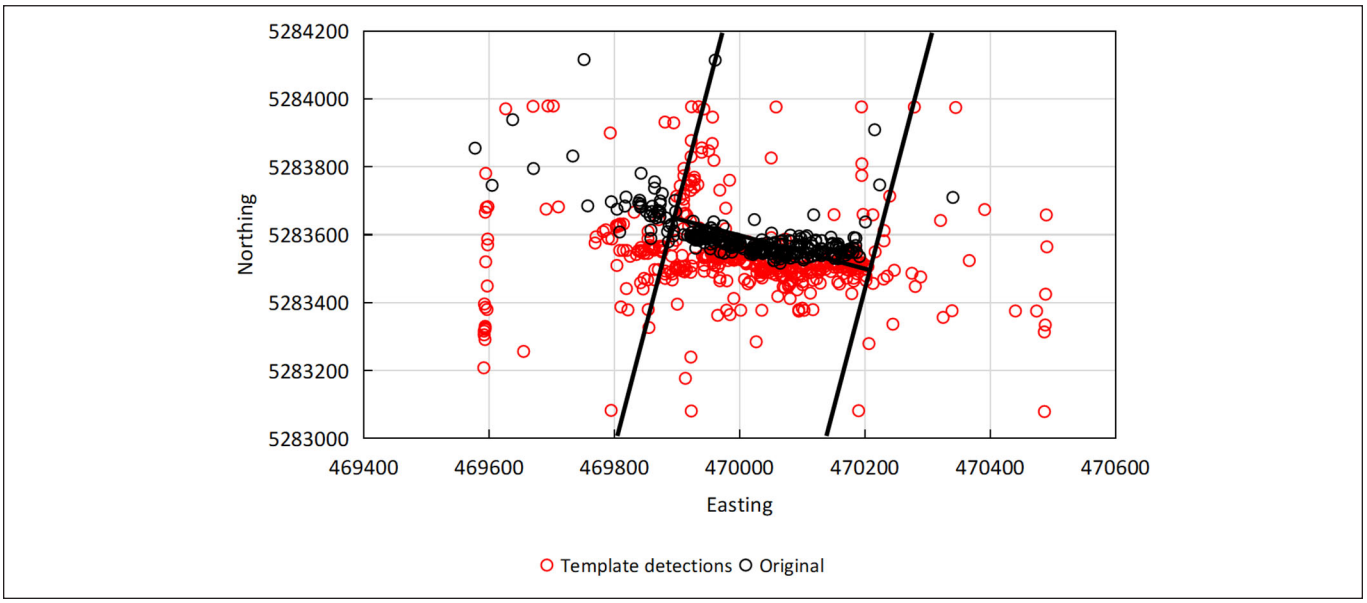


**Figure 9. Locations of original data and locations of template detections for Day 12, with panel outline shown**

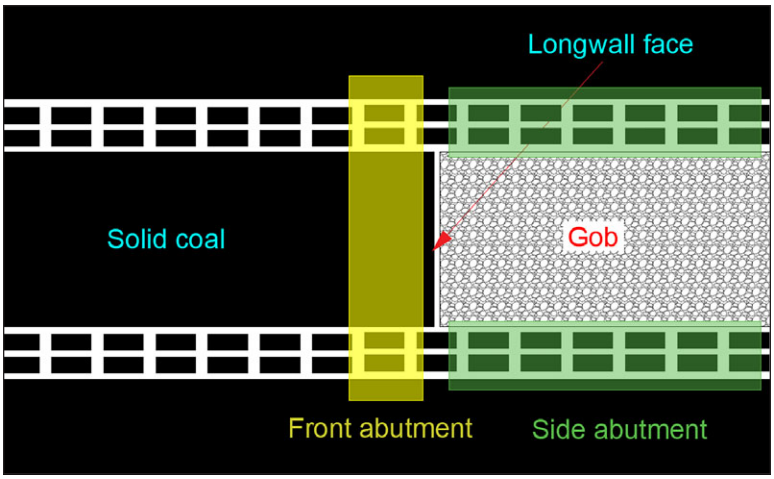


**Figure 10. Typical abutments of longwall mining**

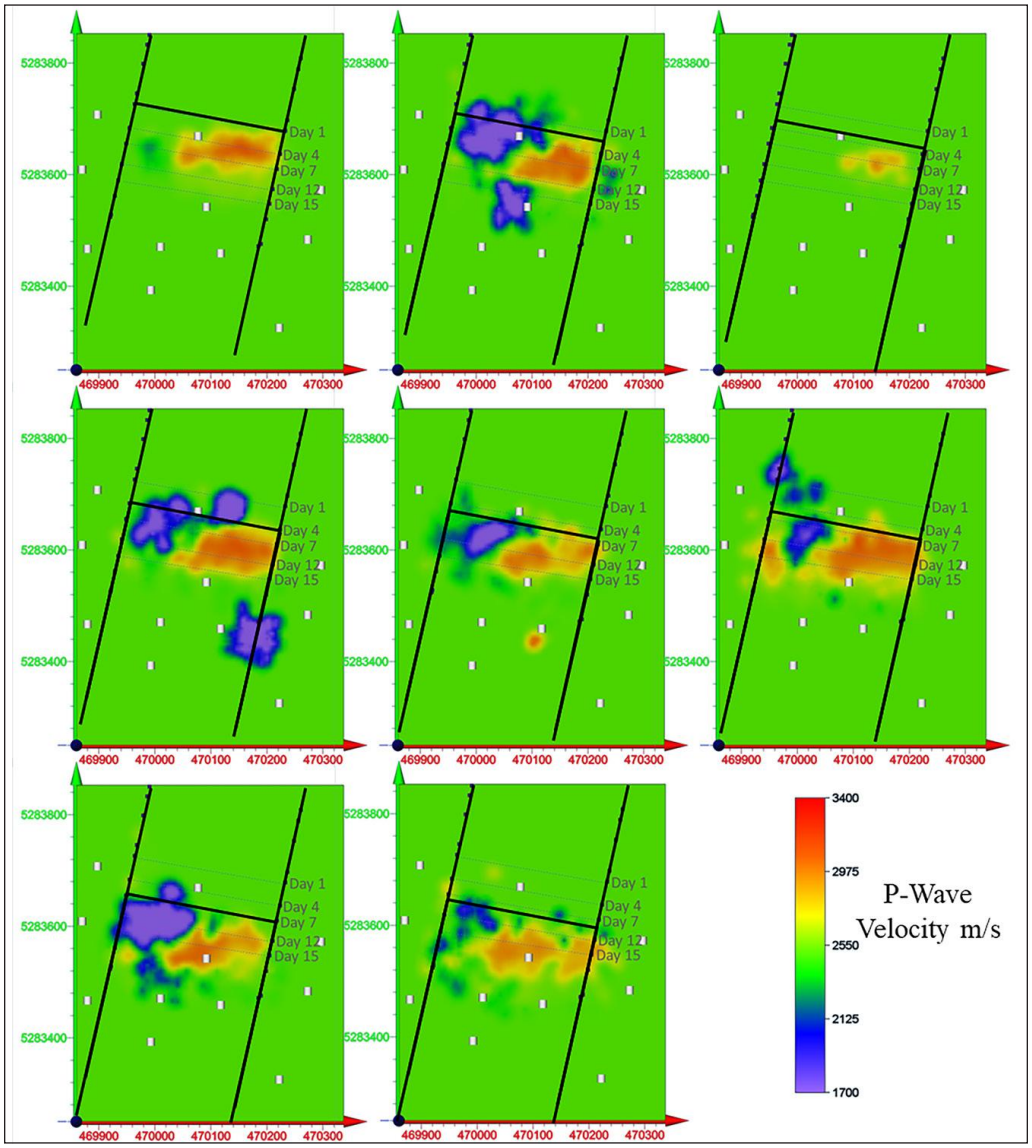


**Figure 11. Horizontal cross sections for each day, taken at the seam elevation, including the face locations for selected days.**

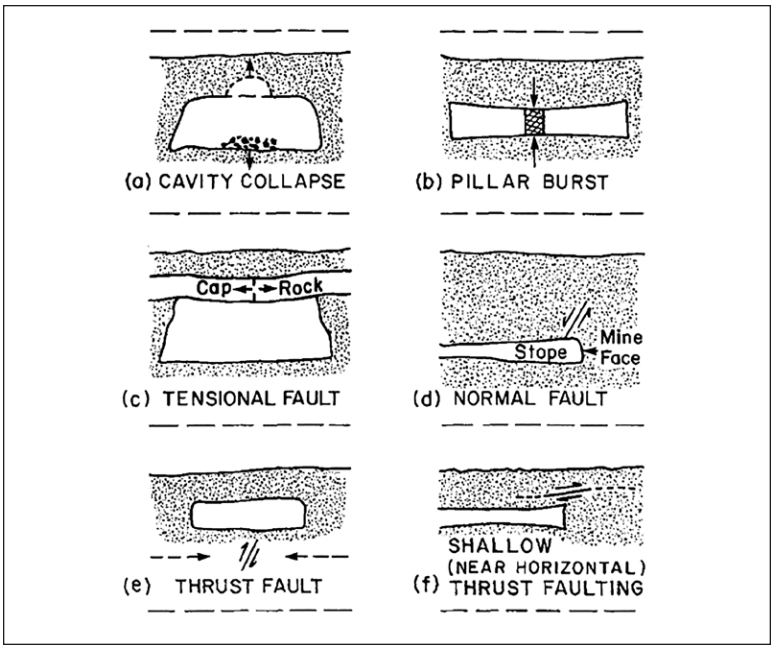


**Figure 12. Schematic diagram of six possible mechanisms of mining-induced microseismic events (Hasegawa et al., 1989)**

## DISCUSSION

This study shows that the template-matching method is feasible in the field of mine microseismic monitoring, which can improve the resolution of passive velocity tomography, and has a good prospect for application in the field of mining-induced hazards prevention and control. However, there are still limitations. The first question is the number of templates that should ideally be used. In the field of natural earthquakes, the number of templates selected by different studies is also variable. Chamberlain et al. (2017) choose 55 initial template events to carry forward to the matched-filter detection stages. Warren-Smith et al. (2018) used 582 detected aftershocks and foreshocks with manual phase picks as templates, which were on 10–40 data channels, across 27 broad-band and short-period sensors. As for mining-induced seismicity, to further analyze the seismicity during the Crandall Canyon Mine collapse on 6 August 2007, Kubacki et al. (2014) selected 55 seismic events as templates to do template matching to pick the low magnitude and low signal-to-noise events.

In this study, 25 waveforms were selected as templates and achieved reasonable results, but the method of how to determine the number of templates was not considered in this paper. In crustal seismology, the waveforms of earthquakes with closely spaced hypocenters tend to be similar, because the similarity of the Green's functions characterizing the source-receiver paths (Gao, 2021). As for microseismic events in a longwall panel, the scale is very small when compared with natural earthquakes, which can further amplify the effects of local changes in structure on the Green's functions, meaning there could be more variation in the waveforms and more templates might be needed to capture events throughout the study area. Another factor for waveform similarity could be the event source mechanism. Hasegawa et al (1989) proposes six possible source mechanisms of mining-induced microseismic events (Figure 12) that will influence the recorded waveforms. Future work could examine the effects of including waveforms from different locations and event types in the template events.

A second limitation is that without additional knowledge of near-seam stratigraphy or the presence of other structures on this longwall panel it is impossible to determine whether the low-velocity zones determined in this study are caused by geological structure, changes in lithology, or lack of sufficient ray coverage.

Thirdly, this study does not realize the earthquake magnitude estimation and focal mechanism analysis at the same time. Magnitude estimation is of great significance to analyze the energy release of mining induced microseismicity and the analysis of the microseismic energy index. Focal mechanism analysis is helpful to analyze mining induced failure mechanisms in surrounding rock, so that it can help to identify mining induced fault-slip and complete rock fracture.

Finally, since only surface geophones were used in the study, there is very little constraint on the depth of the events. Without geophones at the seam level, it is a challenge to correctly determine the vertical location of the events. Additionally, the rapidly changing velocity distribution around the longwall panel, particularly the formation of the gob, also complicates the event location process. All of these limitations provide room for subsequent research, but do not diminish the potential for the use of the template-matching method to add data to the passive seismic tomography process and improve both the spatial and temporal resolution of the images.

## SUMMARY AND CONCLUSIONS

This study demonstrates the potential for template-matching technology implemented with data from a surface microseismic monitoring system mounted above an underground coal longwall panel. Template-matching was shown in this study to be an

effective method to improve the microseismic monitoring results by allowing the detection of low magnitude events, events that are near or below the signal-to-noise ratio, or small events hidden in the signal of larger events. These events are typically too small to be detected by traditional methods in a microseismic monitoring system.

Based on the event locations, travel time and travel distance data, the fast marching method was used to trace the raypaths and a modified SIRT was used for the inversion. The time span for each tomogram is one day. In each tomogram, a high velocity zone can be identified ahead of the face, and in the headgate and tailgate along the gob. These high velocity zones correspond with the distribution of the expected high stress front abutment pressure zone and side abutment pressure zones. The high velocity zones also moved in parallel with the advance of the working face. The passive velocity tomography results based on template-matching method technology can be used to improve the resolution of tomography and shows a good potential in daily mining-induced hazard early warning and control.

## ACKNOWLEDGMENTS

The authors thank Calum Chamberlain in Victoria University of Wellington for his help in studying matched-filter method and EQcorrscan. The authors also thank Anthony Lomax with ALomax Scientific for his help in using the NonLinLoc code, as well as the anonymous reviewers who provided input that strengthened the paper. This research was funded by Key Program of National Natural Science Foundation of China (52130403).

## DISCLAIMER

The findings and conclusions in this report are those of the author(s) and do not necessarily represent the official position of the National Institute for Occupational Safety and Health, Centers for Disease Control and Prevention. Mention of any company or product does not constitute endorsement by NIOSH.

## REFERENCES

Peng, S. (2019). Longwall mining. CRC Press.

Young, R. P., Maxwell, S. C., Urbancic, T. I., & Feignier, B. (1992). Mining-induced microseismicity: monitoring and applications of imaging and source mechanism techniques. Pure and applied geophysics, 139, 697–719.

Trifu, C. I., & Suorineni, F. T. (2009). Use of microseismic monitoring for rockburst management at Vale Inco mines. In Proceedings of 7th International Symposium on Rockburst and Seismicity in Mines (RASIM7),1105–1114.

Wepfer, W. W., & Christensen, N. I. (1991). A seismic velocity-confining pressure relation, with applications. International Journal of Rock Mechanics and Mining Sciences & Geomechanics Abstracts, 28(5), 451–456.

Khaksar, A., Griffiths, & McCann. (2001). Compressional—and shear—wave velocities as a function of confining stress in dry sandstones. Geophysical Prospecting, 47(4), 487–508.

Zheng, G. P., Zhao, X. D., Liu, J. P., & Li, Y. H. (2009). Experimental study on change in acoustic wave velocity when rock is loading. Journal of Northeastern University (Natural Science), 30(8), 1197–1200.

Rezaei, M., Hossaini, M. F., & Majdi, A. (2015). Determination of longwall mining-induced stress using the strain energy method. Rock Mechanics and Rock Engineering, 48, 2421–2433.

Xu, W. Q. (2012). Studies on monitoring technology of mining space surrounding rock stress and its application. China University Mining and Technology, Xuzhou, China.

Luxbacher, K., Westman, E., Swanson, P., & Karfakis, M. (2008). Three-dimensional time-lapse velocity tomography of an underground longwall panel. International Journal of Rock Mechanics and Mining Sciences, 45(4), 478–485.

Li G. Y. (2013). Study of The Synchronized Correlation between Stress and Ultrasonic Velocity of Sandstone in Real Time. Lanzhou University, Lanzhou, China.

Nur, A., & Simmons, G. (1969). Stress—induced velocity anisotropy in rock: An experimental study. Journal of Geophysical Research, 74(27), 6667–6674.

Maxwell, S. C., & Young, R. P. (1992). Sequential velocity imaging and microseismic monitoring of mining-induced stress change. Pure and Applied Geophysics, 139, 421–447.

Westman, E. C. (1993). Characterization of structural integrity and stress state via seismic methods: a case study. In Proceedings of the 12th International Conference on Ground Control in Mining. West Virginia Univ., Morgantown, WV, USA, 322–328.

Ma, X., Westman, E., Counter, D., Malek, F., & Slaker, B. (2020). Passive seismic imaging of stress evolution with mining-induced seismicity at hard-rock deep mines. Rock Mechanics and Rock Engineering, 53, 2789–2804.

Ghaychi Afrouz, S. (2020). Seismic Wave Velocity Variations in Deep Hard Rock Underground Mines by Passive Seismic Tomography. Virginia Tech.

Gibowicz, G. (2012). Seismicity in Mines. Birkhäuser.

Mendecki, A. J. (1996). Seismic Monitoring in Mines. Springer Science & Business Media.

Knoll, P. (1989). The Fluid-induced Tectonic Rockburst of March 13, 1989 in the “Werra” potash mining district of the GDR (first Results). In ISRM International Symposium, 99, 239–245.

Pechmann, J. C., Walter, W. R., Nava, S. J., & Arabasz, W. J. (1996). The February 3, 1995, ML 5.1 seismic event in the Trona mining district of southwestern Wyoming. Seismological Research Letters, 66(3), 25–34.

Chambers, D. J., Koper, K. D., Pankow, K. L., & McCarter, M. K. (2015). Detecting and characterizing coal mine related seismicity in the Western US using subspace methods. Geophysical Journal International, 203(2), 1388–1399.

Chamberlain, C. J., Boese, C. M., & Townend, J. (2017). Cross-correlation-based detection and characterisation of microseismicity adjacent to the locked, late-interseismic Alpine Fault, South Westland, New Zealand. Earth and Planetary Science Letters, 457, 63–72.

Yin X. X. (2018). Research on seismic sequence completeness based on template matching method and the double-difference location. Lanzhou Institute of Seismology, China Earthquake Administration.

Yin X. Z. (2019). Spatial-temporal evolution and fault zone imaging before and after the Wenchuan Earthquake using the waveform matched filtering method. Institute of Geology, China Earthquake Administration.

Li N., Zhang X., Huang B.X., & Tan Y. Y. (2018). Automatic detection model of acoustic emission events of coal and rock based on waveforms correlation. Journal of China Coal Society, 43(7): 1893–1901.

Peng, Z., & Zhao, P. (2009). Migration of early aftershocks following the 2004 Parkfield earthquake. Nature Geoscience, 2(12), 877–881.

Spottiswoode, S. M., & Milev, A. M. (1998). The use of waveform similarity to define planes of mining-induced seismic events. Tectonophysics, 289(1-3), 51–60.

Chambers, D. J. A. (2015). Application of subspace methods to detect and characterize coal mine related seismicity in the western United States. The University of Utah.

Boltz, M. S., Chambers, D. J. A., & Hanson, D. R. (2018, June). Evaluating seismicity at underground coal mines using temporary surface geophone deployments. In ARMA US Rock Mechanics/Geomechanics Symposium (pp. ARMA-2018). ARMA.

Johnson, S. W., Chambers, D. J., Boltz, M. S., & Koper, K. D. (2021). Application of a convolutional neural network for seismic phase picking of mining-induced seismicity. Geophysical journal international, 224(1), 230–240.

Slinkard, M., Schaff, D., Mikhailova, N., Heck, S., Young, C., & Richards, P. G. (2014). Multistation validation of waveform correlation techniques as applied to broad regional monitoring. Bulletin of the Seismological Society of America, 104(6), 2768–2781.

Lomax, A., Virieux, J., Volant, P., & Berge-Thierry, C. (2000). Probabilistic earthquake location in 3D and layered models: Introduction of a Metropolis-Gibbs method and comparison with linear locations. Advances in seismic event location, 101–134.

Lomax, A., Michelini, A., Curtis, A., & Meyers, R. A. (2009). Earthquake location, direct, global-search methods. Encyclopedia of complexity and systems science, 5, 2449–2473.

Tarantola, A. (1987). Inverse problem theory and methods for model parameter estimation. Society for Industrial and Applied Mathematics.

Tarantola, A., & Valette, B. (1982). Inverse problems= quest for information. Journal of geophysics, 50(1), 159–170.

Podvin, P., & Lecomte, I. (1991). Finite difference computation of traveltimes in very contrasted velocity models: a massively parallel approach and its associated tools. Geophysical Journal International, 105(1), 271–284.

Warren-Smith, E., Fry, B., Kaneko, Y., & Chamberlain, C. J. (2018). Foreshocks and delayed triggering of the 2016 MW7. 1 Te Araroa earthquake and dynamic reinvigoration of its aftershock sequence by the MW7. 8 Kaikōura earthquake, New Zealand. Earth and Planetary Science Letters, 482, 265–276.

Kubacki, T., Koper, K. D., Pankow, K. L., & McCarter, M. K. (2014). Changes in mining—induced seismicity before and after the 2007 Crandall Canyon Mine collapse. Journal of Geophysical Research: Solid Earth, 119(6), 4876–4889.

Gao, D. (2021). Comprehensive study of seismic waveform similarity: applications to reliable identification of repeating earthquakes and investigations of detailed source process of induced seismicity. University of Victoria.

Hasegawa, H. S., Wetmiller, R. J., & Gendzwill, D. J. (1989). Induced seismicity in mines in Canada—an overview. Pure and Applied Geophysics, 129, 423–453.

# PROCEEDINGS OF THE 43rd International Conference ON GROUND CONTROL IN MINING

## ICGCM 2024

Edited by

Ted Klemetti | Rudrajit Mitra | Michael Murphy | Kyle Perry | Ihsan Berk Tulu

SME Society for Mining, Metallurgy & Exploration®

**Society for Mining, Metallurgy & Exploration (SME)**
12999 E. Adam Aircraft Circle
Englewood, Colorado, USA 80112
(303) 948-4200 / (800) 763-3132
www.smenet.org

**The Society for Mining, Metallurgy & Exploration (SME)** is a professional society whose more than 15,000 members represents all professionals serving the minerals industry in more than 100 countries. SME members include engineers, geologists, metallurgists, educators, students and researchers. SME advances the worldwide mining and underground construction community through information exchange and professional development.



ebook ISBN 978-0-87335-516-2